

Computation of ground-state properties in molecular systems: back-propagation with auxiliary-field quantum Monte Carlo

Mario Motta¹ and Shiwei Zhang¹

¹*Department of Physics, College of William and Mary, Williamsburg, Virginia 23187-8795, USA*

We address the computation of ground-state properties of chemical systems and realistic materials within the auxiliary-field quantum Monte Carlo method. The phase constraint to control the fermion phase problem requires the random walks in Slater determinant space to be open-ended with branching. This in turn makes it necessary to use back-propagation (BP) to compute averages and correlation functions of operators that do not commute with the Hamiltonian. Several BP schemes are investigated and their optimization with respect to the phaseless constraint is considered. We propose a modified BP method for the computation of observables in electronic systems, discuss its numerical stability and computational complexity, and assess its performance by computing ground-state properties for several substances, including constituents of the primordial terrestrial atmosphere and small organic molecules.

I. INTRODUCTION

The quantitative study of molecular systems requires accurate and efficient calculations of ground-state properties and correlation functions. For many applications, this task corresponds to solving the electronic many-body Schrödinger equation within the Born-Oppenheimer approximation, and computing observables and correlation functions as ground-state averages of suitable operators.

The last decades have witnessed the development of a variety of numerical techniques to address the solution of the many-body Schrödinger equation, ranging in quality from the mean-field Hartree-Fock (HF) to the exact full configuration interaction (FCI). The coupled-cluster (CC) and quantum Monte Carlo (QMC) methods [1–4] are two examples of techniques that incorporate electronic correlations beyond the HF level to achieve a better description of the system.

QMC methods provide a non-perturbative treatment of interacting many-body systems, typically with excellent accuracy. Their computational complexity scales as a low power of the system size. With the advent of powerful computational resources, they are becoming increasingly valuable for unveiling the properties of quantum many-particle models and real materials [4–6].

A broad class of projector QMC methods are based on the mapping between the imaginary-time evolution and a suitable stochastic process [3]. Projector QMC methods differ from each other by the choice of the mapping and by the approximation schemes employed to control the well-known sign problem [7]. In particular the QMC method with the longest history in electronic structure is the real space fixed-node diffusion Monte Carlo (DMC), which samples the many-body ground-state function in the configurational space of the studied system [3, 4, 8].

The more recent auxiliary-field quantum Monte Carlo (AFQMC) method is an alternative and complementary QMC approach, based on the mapping between the imaginary-time evolution and a stochastic process taking place in a non-orthogonal manifold of Slater determinants [9]. AFQMC has provided excellent results for

ground-state energies and energy differences in solids and molecules [10–17]. While AFQMC has been extensively applied in lattice models to calculate both ground-state energies and other observables and correlation functions [18–20], the calculation of ground-state properties other than the total energy has to date not been systematically investigated in molecules and other realistic materials.

In the present work, we formulate and implement a back-propagation (BP) technique [21, 22] for calculating ground-state properties of realistic electronic Hamiltonians with the AFQMC method. We show that, under the formalism adopted in electronic systems, which often involves a phaseless constraint, a simple refinement of the original back-propagation [22] leads to substantial improvement in the quality of the computed observables. The theoretical basis for the improvement is discussed. We then give a detailed description of our algorithm, and consider its numeric stability and computational complexity. To assess the accuracy of the methodology, we compute ground-state averages of one-body operators and two-body correlation functions for several molecules, including constituents of the primordial terrestrial atmosphere and small organic molecules. Results are compared with FCI and CC where available.

The remainder of this paper is organized as follows. The AFQMC method for total energy calculations (without back-propagation) is outlined in Sec. II. The back-propagation technique and our implementation as well as technical improvements for electronic systems are then described in Sec. III. Results are presented in Sec. IV and conclusions are drawn in Sec. V.

II. THE AFQMC METHOD

We first provide a brief overview of the AFQMC method [9, 23], to establish the notation and present the concepts relevant to the formulation of the back-propagation algorithm. The hamiltonian of a many-electron system with spin-independent external potential

and two-body interactions can be written as

$$\begin{aligned}\hat{H} &= \sum_{ij,\sigma} T_{ij} \hat{a}_{i\sigma}^\dagger \hat{a}_{j\sigma} + \sum_{ijkl,\sigma\tau} \frac{V_{ijkl}}{2} \hat{a}_{i\sigma}^\dagger \hat{a}_{j\tau}^\dagger \hat{a}_{k\tau} \hat{a}_{l\sigma} = \\ &= \hat{H}_1 + \hat{H}_2\end{aligned}\quad (1)$$

where the creation and annihilation operators $\hat{a}_{i\sigma}^\dagger$, $\hat{a}_{j\sigma}$ are related to an orthonormal set of one-electron orbitals $\{\varphi_i(\mathbf{r})\}_{i=1}^M$, and the one-body and two-body matrix elements T_{ij} , V_{ijkl} are generated by quantum chemistry softwares (or via a downfolding procedure using Kohn-Sham orbitals [24]).

The AFQMC method is based on the observation that the ground state Ψ_0 of (1) can be expressed as

$$|\Psi_0\rangle = \lim_{\beta \rightarrow \infty} e^{-\beta(\hat{H}-E_0)} |\Psi_I\rangle \quad (2)$$

where Ψ_I is any initial wavefunction having non-zero overlap with Ψ_0 , and E_0 the ground-state energy of \hat{H} . (In an AFQMC calculation E_0 is replaced by a trial energy which can be estimated adaptively.) Applying the propagator $e^{-\beta(\hat{H}-E_0)}$ to Ψ_I requires the discretization of the imaginary-time propagation

$$e^{-\beta(\hat{H}-E_0)} = \left(e^{-\delta\beta(\hat{H}-E_0)} \right)^n, \quad \delta\beta = \frac{\beta}{n}, \quad (3)$$

and the combined use of the Trotter-Suzuki decomposition [25, 26]

$$e^{-\delta\beta\hat{H}} = e^{-\frac{\delta\beta}{2}\hat{H}_1} e^{-\delta\beta\hat{H}_2} e^{-\frac{\delta\beta}{2}\hat{H}_1} + \mathcal{O}(\delta\beta^3) \quad (4)$$

and the Hubbard-Stratonovich transformation [27, 28]

$$e^{-\delta\beta(\hat{H}-E_0)} = \int d\mathbf{x} p(\mathbf{x}) \hat{B}(\mathbf{x}) + \mathcal{O}(\delta\beta^2). \quad (5)$$

In (5), the operators $\hat{B}(\mathbf{x})$ are given by

$$\hat{B}(\mathbf{x}) = e^{-\frac{\delta\beta}{2}\hat{H}_1} \prod_{\gamma} e^{\sqrt{\delta\beta}x_{\gamma}\hat{v}_{\gamma}} e^{-\frac{\delta\beta}{2}\hat{H}_1} e^{\delta\beta E_0}, \quad (6)$$

the operators \hat{v}_{γ} , typically obtained through a modified Cholesky decomposition of the two-body tensor V_{ijkl} [15], are such that $\hat{H}_2 = -\frac{1}{2}\sum_{\gamma}\hat{v}_{\gamma}^2$, and $p(\mathbf{x})$ is the normal probability distribution. Equations (3), (4) and (5) yield the following stochastic representation of the ground-state wavefunction:

$$e^{-n\delta\beta(\hat{H}-E_0)} |\Psi_I\rangle \simeq \int d\mathbf{X} p(\mathbf{X}) |\Psi_n(\mathbf{X})\rangle \quad (7)$$

where $\mathbf{X} = (\mathbf{x}_{n-1} \dots \mathbf{x}_0)$ is a path of auxiliary fields and $|\Psi_n(\mathbf{X})\rangle = \hat{B}(\mathbf{x}_{n-1}) \dots \hat{B}(\mathbf{x}_0) |\Psi_I\rangle$. We will frequently write Ψ_n in place of $\Psi_n(\mathbf{X})$ to reduce clutter.

The practical usefulness of (7) rests upon Thouless's theorem, ensuring that the operators $\hat{B}(\mathbf{x}_i)$, acting on a Slater determinant Ψ_I , yield another Slater determinant

Ψ_n [23]. Equation (7) maps the imaginary-time projection onto a stochastic process in the manifold of Slater determinants, which can be efficiently simulated thanks to the well-known algebraic properties of these many-body states [23]. Such mapping gives rise to an algorithmic procedure via the so-called free-projection AFQMC, with computational cost scaling as $\mathcal{O}(M^2N + N^3)$ for propagation and possibly $\mathcal{O}(M^4)$ for computing two-body expectation values (for the energy, the scaling can be reduced to $\mathcal{O}(M^2N^2)$ or better.)

A. Importance sampling

The straightforward free-projection AFQMC manifests a well-known exponential increase in statistical fluctuations with the projection time $n\delta\beta$ [29]. This is the sign problem [7], which for general Coulomb interactions turns into a phase problem [9]. The problem is controlled by combining an importance sampling procedure, briefly overviewed below, with suitable approximations.

The starting point of the importance sampling is performing a shift of the auxiliary fields in (7)

$$\begin{aligned}e^{-n\delta\beta(\hat{H}-E_0)} \frac{|\Psi_I\rangle}{\langle\Psi_T|\Psi_I\rangle} &\simeq \int d\mathbf{X} p(\mathbf{X} - \bar{\mathbf{X}}) \frac{|\Psi_n(\mathbf{X} - \bar{\mathbf{X}})\rangle}{\langle\Psi_T|\Psi_I\rangle} \\ &= \int d\mathbf{X} p(\mathbf{X}) W_n(\mathbf{X}, \bar{\mathbf{X}}) \frac{|\Psi_n\rangle}{\langle\Psi_T|\Psi_n\rangle}\end{aligned}\quad (8)$$

where Ψ_T is a trial wavefunction used to guide the simulation, which can be different from Ψ_I if desired, the vector $\bar{\mathbf{X}}$ can be complex-valued, and the weights $W_n(\mathbf{X}, \bar{\mathbf{X}})$ are defined in terms of the importance function

$$I(\mathbf{x}, \bar{\mathbf{x}}, \Psi) = \frac{p(\mathbf{x} - \bar{\mathbf{x}})}{p(\mathbf{x})} \frac{\langle\Psi_T|\hat{B}(\mathbf{x} - \bar{\mathbf{x}})|\Psi\rangle}{\langle\Psi_T|\Psi\rangle} \quad (9)$$

as

$$W_n(\mathbf{X}, \bar{\mathbf{X}}) = \prod_{i=0}^{n-1} I(\mathbf{x}_i, \bar{\mathbf{x}}_i, \Psi_i). \quad (10)$$

The components $\bar{\mathbf{x}}_i$ of $\bar{\mathbf{X}}$ are chosen [22] to minimize fluctuations in the importance function to first order in $\delta\beta$, and read

$$(\bar{\mathbf{x}}_i)_{\gamma} = -\sqrt{\delta\beta} \frac{\langle\Psi_T|\hat{v}_{\gamma}|\Psi_i\rangle}{\langle\Psi_T|\Psi_i\rangle}. \quad (11)$$

Although the vectors $\bar{\mathbf{x}}_i$ drive the random walk towards the region of the complex plane where $\langle\Psi_T|\Psi\rangle$ is large, the importance sampling, which is a similarity transformation, is not able to stabilize the random walk of Slater determinants. The phase problem manifests itself in two aspects after importance sampling. First, walkers whose overlap with Ψ_T is small in magnitude cause large fluctuations in the weights and their contributions to the estimators. Second, the weights in (8) are complex and these quantities diffuse in the complex plane, resulting in cancelling signals in the Monte Carlo estimators of ground-state properties and correlation functions [23].

B. The phaseless approximation

To achieve complete control of the phase problem, we rely on a phaseless approximation, where the importance function is modified as follows:

$$I(\mathbf{x}, \bar{\mathbf{x}}, \Psi) \simeq e^{\delta\beta[E_0 - \text{Re}(E_L)]} \times \max(0, \cos(\Delta\theta)) , \quad (12)$$

the local energy E_L and $\Delta\theta$ being

$$E_L(\Psi) = \frac{\langle \Psi_T | \hat{H} | \Psi \rangle}{\langle \Psi_T | \Psi \rangle} , \quad (13)$$

$$\Delta\theta = \text{Arg} \frac{\langle \Psi_T | \hat{B}(\mathbf{x} - \bar{\mathbf{x}}) | \Psi \rangle}{\langle \Psi_T | \Psi \rangle} .$$

The first factor in Eq. (12), corresponding to the real local energy approximation, turns weights into real and positive quantities. The second, corresponding to a projection after the proper gauge condition has been imposed with the choice of $\bar{\mathbf{x}}$ in Eq. (11), prevents the scalar products $\langle \Psi_T | \Psi \rangle$ from undergoing a rotationally-invariant random walk in the complex plane, thus avoiding a finite concentration of walkers at the origin.

In Eq. (12) the ‘cos’ can be replaced by a line constraint or a Gaussian weight [9, 30]. These share the same basic idea as above and were seen to give similar results for the computed ground-state energy in the tests in jellium [9] and repulsive Bose systems with modest interactions [31]. Regarding the first part, it was found that the imaginary part of the local energy accumulates slowly and can be carried for extended projection time in electronic systems; however this seems to have little effect on the computed ground state energy.

C. The phaseless AFQMC algorithm for total energy

The resulting algorithm, the phaseless AFQMC, can be summarized by the following sequence of operations:

1. N_w walkers, labeled by k , are initialized at $\Psi_{0,k} \equiv \Psi_I$, each with weight $W_{0,k} \equiv 1$. (If a multi-determinant Ψ_I is used, the different determinants can be sampled according to their weights in Ψ_I .)
2. For each k , $\mathbf{x}_{i,k}$ is sampled, the walker is updated as

$$\Psi_{i+1,k} = \hat{B}((\mathbf{x} - \bar{\mathbf{x}})_{i,k}) \Psi_{i,k}$$

and the weight as

$$W_{i+1,k} = I(\mathbf{x}_{i,k}, \bar{\mathbf{x}}_{i,k}, \Psi_{i,k}) W_{i,k}$$

3. Step 2 is iterated n times, and Eq. (8) is realized in a Monte Carlo sense as a weighted average as $\mathcal{N} \sum_{k=1}^{N_w} W_{n,k} \frac{|\Psi_{n,k}\rangle}{\langle \Psi_T | \Psi_{n,k} \rangle}$, where \mathcal{N} is a normalization constant that depends on the trial energy E_0 and the sum of the weights.

4. Periodically, the walkers $\{\Psi_{i,k}\}$ are stabilized, for example, using a modified Gram-Schmidt procedure [23]. Additionally, the weights can be reorganized using a branching algorithm [9].

Additional algorithmic improvements enhance the efficiency and stability of AFQMC calculations, for instance subtracting a mean-field contribution to the two-body part of the Hamiltonian prior to the HS transformation [10, 14, 29] and bounding weights and force biases [14]. This approach was successfully applied to a broad number of quantum chemistry [6, 32, 33] and solid state physics systems [22, 24].

III. COMPUTATION OF OBSERVABLES AND CORRELATION FUNCTIONS IN AFQMC

The importance sampling transformation provides a stochastic representation of the ground-state wavefunction as a weighted average of rescaled Slater determinants, and gives the possibility of computing the mixed estimator

$$A_{\text{mix}} = \frac{\langle \Psi_T | \hat{A} | \Psi_0 \rangle}{\langle \Psi_T | \Psi_0 \rangle} \quad (14)$$

of an observable \hat{A} as a weighted average

$$A_{\text{mix}} \simeq \frac{1}{\sum_k W_{n,k}} \sum_k W_{n,k} \frac{\langle \Psi_T | \hat{A} | \Psi_{n,k} \rangle}{\langle \Psi_T | \Psi_{n,k} \rangle} , \quad (15)$$

where the rescaled matrix elements can be evaluated in a manner similar to the total energy. Unless $[\hat{A}, \hat{H}] = 0$, the mixed estimator of \hat{A} is biased by the trial wavefunction Ψ_T used for importance sampling. A simple method to approximately remove the bias in the mixed estimator is the extrapolation

$$A_{\text{ex}} = 2A_{\text{mix}} - A_T , \quad A_T = \frac{\langle \Psi_T | \hat{A} | \Psi_T \rangle}{\langle \Psi_T | \Psi_T \rangle} . \quad (16)$$

Expectation values obtained through the extrapolated estimator, however, still contain bias from the choice of the trial wavefunction which is difficult to assess. Indeed, because the trial wave functions tend to be quite poor (often a single Slater determinant) in AFQMC, the extrapolated estimator can often be worse than the mixed estimator [22].

A. Phaseless back-propagation (BP-PhL)

In order to overcome these restrictions, Zhang and coworkers proposed a back-propagation (BP) technique [21, 22] in the framework of AFQMC. The starting point of the BP algorithm is the observation that, for large n and m ,

$$A_{\text{BP}} \equiv \frac{\langle \Psi_T | e^{-m\delta\beta\hat{H}} \hat{A} e^{-n\delta\beta\hat{H}} | \Psi_I \rangle}{\langle \Psi_T | e^{-(m+n)\delta\beta\hat{H}} | \Psi_I \rangle} \simeq \frac{\langle \Psi_0 | \hat{A} | \Psi_0 \rangle}{\langle \Psi_0 | \Psi_0 \rangle} . \quad (17)$$

The measurement above reduces to the mixed estimator when $m = 0$. Inserting (7) into (17) yields

$$A_{\text{BP}} = \frac{\int d\mathbf{X} p(\mathbf{X}) \langle \Phi_m(\mathbf{X}) | \hat{A} | \Psi_n(\mathbf{X}) \rangle}{\int d\mathbf{X} p(\mathbf{X}) \langle \Phi_m(\mathbf{X}) | \Psi_n(\mathbf{X}) \rangle} \quad (18)$$

with $\mathbf{X} = (\mathbf{x}_{n+m-1} \dots \mathbf{x}_0)$ and

$$|\Phi_m(\mathbf{X})\rangle = \hat{B}(\mathbf{x}_n)^\dagger \dots \hat{B}(\mathbf{x}_{n+m-1})^\dagger |\Psi_T\rangle. \quad (19)$$

As before, we will use the abbreviation Φ_m to denote $\Phi_m(\mathbf{X})$. Applying the shift on the path segment from $n+1$ to m in the forward direction, i.e., viewing the entire path \mathbf{X} as a forward projection from $|\Psi_I\rangle$ and performing the importance sampling transformation of Sec. II A, yields

$$A_{\text{BP}} = \frac{\int d\mathbf{X} p(\mathbf{X}) W_{n+m}(\mathbf{X}, \bar{\mathbf{X}}) \frac{\langle \Phi_m | \hat{A} | \Psi_n \rangle}{\langle \Phi_m | \Psi_n \rangle}}{\int d\mathbf{X} p(\mathbf{X}) W_{n+m}(\mathbf{X}, \bar{\mathbf{X}})}. \quad (20)$$

In a calculation with importance sampling, the quantity A_{BP} is thus estimated as the following weighted average

$$A_{\text{BP}} \simeq \frac{1}{\sum_k W_{n+m,k}} \sum_k W_{n+m,k} \frac{\langle \Phi_{m,k} | \hat{A} | \Psi_{n,k} \rangle}{\langle \Phi_{m,k} | \Psi_{n,k} \rangle}, \quad (21)$$

with

$$|\Psi_{n,k}\rangle = \hat{B}((\mathbf{x} - \bar{\mathbf{x}})_{n-1,k}) \dots \hat{B}((\mathbf{x} - \bar{\mathbf{x}})_{0,k}) |\Psi_I\rangle \quad (22)$$

which is the usual forward projection in total energy calculations, and

$$|\Phi_{m,k}\rangle = \hat{B}^\dagger((\mathbf{x} - \bar{\mathbf{x}})_{n,k}) \dots \hat{B}^\dagger((\mathbf{x} - \bar{\mathbf{x}})_{n+m-1,k}) |\Psi_T\rangle \quad (23)$$

which uses the auxiliary-field path in the backward direction for projection. Note that the matrix elements in Eq. (21) can be efficiently evaluated for both one- and two-body operators [23]. One important advantage of the AFQMC method with BP is that the Monte Carlo samples, $\{|\Phi_m|\}$ and $\{|\Psi_n|\}$, are non-orthogonal, which allow essentially any correlation functions to be computed conveniently in electronic systems.

The back-propagation technique, illustrated in Figure 1, makes use of auxiliary fields configurations from different segments of the random walk to project the trial wavefunction also at the left of \hat{A} . In the absence of any constraint for controlling the sign or phase problem, this estimator approaches the exact expectation value as the number m of back-propagation steps is increased. When a constraint is applied in the forward direction, the backward paths do not satisfy the same constraint so that the BP estimators are approximate and not variational.

B. Improved back-propagation algorithm - path restoration (BP-PRes)

The BP approach described above has been successfully applied to a variety of lattice models [18, 19, 29], in

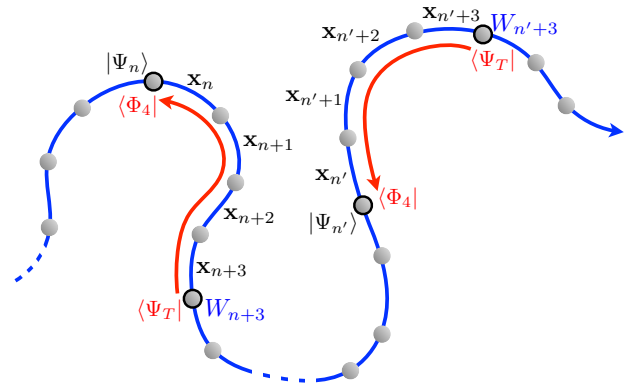


FIG. 1. (color online) Pictorial illustration of the back-propagation technique. For each walker k , $|\Psi_{n,k}\rangle$ is computed at a time step n , $|\Phi_{m,k}\rangle$ is computed between the time steps n and $n+m$, and the weight $W_{n+m,k}$ at the time step $n+m$. Here the path for one walker is shown for two BP segments with $m = 4$ back-propagation steps in each. Evaluation of A_{BP} is performed periodically during the simulation following Eq. (21).

which the local interactions induce “only” a sign problem and the phaseless approximation reduces to the simpler constrained-path approximation of $\langle \Psi_T | \Psi \rangle > 0$. In the presence of a phase problem when the phaseless approximation is required, the simple approach of directly using the phaseless paths has been used in weakly interacting boson gases [31] and dense homogeneous electron gases [34, 35].

In model systems where the one-body propagator in Eq. (6) is real (or only has a trivial phase uncoupled to the random fields [36]), there is no ambiguity on how to formulate the BP, since the only role of the constraint is to terminate a path in the forward direction when the constraint is violated. In the general case when $\hat{B}(\mathbf{x})$ is complex, there are additional modifications to the weights of the path (beyond the importance sampling transformation, whose effect is properly accounted for by using the “retarded” weight in Eq. (21)). The importance function $I(\mathbf{x}, \bar{\mathbf{x}}, \Psi)$ is equal to the exponential of the local energy, $e^{\delta\beta(E_0 - E_L(\Psi))}$, up to terms of order $\delta\beta^{\frac{3}{2}}$ [34]. The real local energy approximation in Eq. (12) removes the imaginary part of the local energy from the importance function, leaving positive weights. The cosine projection multiplies the importance function by another positive factor, to remove the “two-dimensional” nature of the random walk (in the complex plane of overlaps).

The effect of the above two steps is to alter the weight in the forward direction. The accumulation of their effect can be to terminate certain paths; once this occurs it cannot be recovered in the backward direction. The numerical modification to the weight, however, can be restored for BP among the paths that survive from step n to step $(n+m)$ in Eqs. (20) and (21). Given that the backward direction would be exact if no phaseless projection on the weight had been applied in the forward

direction (although this obviously would re-introduce the phase problem), it is reasonable to restore the paths as much as possible in the backward direction, by undoing the extra weight modifications that arose from the phaseless approximation.

We will call the simple BP procedure without undoing any weights BP-PhL (phaseless), and the procedure which restores the weight projection and the phase of the local energy in the BP direction BP-PRes (path restoration). This distinction only exists when there is a genuine phase problem from a complex $\hat{B}(\mathbf{x})$ with phase factors coupled to \mathbf{x} . (As mentioned, when $\hat{B}(\mathbf{x})$ is real, both of these approaches will revert back to the standard BP formulated for the case of the sign problem [21].) In weakly interacting systems, the two approaches are expected to be similar, since the effect of the phase projection is weak.

In the BP-PRes algorithm, we replace the BP estimator with

$$A_{\text{BP}} \simeq \frac{1}{\sum_k \tilde{W}_{n+m,k}} \sum_k \tilde{W}_{n+m,k} \frac{\langle \Phi_{m,k} | \hat{A} | \Psi_{n,k} \rangle}{\langle \Phi_{m,k} | \Psi_{n,k} \rangle}, \quad (24)$$

where

$$\tilde{W}_{n+m,k} = W_{n,k} \prod_{j=n}^{n+m} e^{\delta\beta(E_0 - E_L(\Psi_j))}. \quad (25)$$

This is realized by remembering the phase factor from $\text{Im}(E_L)$ and the cosine projection factor in Eq. (12) along the path from step n to step $(n+m)$ for each walker, and multiplying $W_{n+m,k}$ by the former and dividing it by the latter, to give $\tilde{W}_{n+m,k}$ for the weight in the BP estimator in Eq. (24). As we illustrate in the next Section, this modification leads to significant improvement.

We stress that it is only in the backward direction that the restoration of the path occurs, i.e., retaining the imaginary part of the local energy and undoing the cosine projection. This procedure increases the fluctuation in the BP estimators. However, the BP algorithm is only applied for a finite time $\beta_{\text{BP}} = m\delta\beta$, which must be kept as small as possible to avoid population instability, i.e., the population at step $(n+m)$ should come from ancestors which make up a significant of the population at step n . As such, undoing the phase projection does not cause fundamental instabilities in the algorithm. As mentioned, the phase in the local energy can typically be carried for much longer than β_{BP} without noticeable effect. The restoring of the projection is only for the paths that survive in the forward direction and thus the additional weight factors are well regulated.

C. Additional algorithmic discussions

1. Numeric stabilization and computational cost

Periodic stabilization of the random walkers is necessary in the propagation in the forward direction to prevent the single-particle orbitals in the Slater determinant

from losing orthogonality from numerical noise (collapsing to a bosonic state). This is often done with a modified Gram-Schmidt decomposition, $\Psi = UDV$, where U is an $M \times N$ matrix which contains orthonormal orbitals, D is an $N \times N$ diagonal matrix, and V is an upper triangular matrix whose diagonal elements are 1.

Similarly, in the backward direction, when we propagate the trial wave function by Eq. (19) or (23), stabilization is necessary. This can be handled straightforwardly following the same procedure as in the forward direction. Assuming that Ψ_T is a Slater determinant (the case of multideterminants is discussed below), the application of the propagators \hat{B}^\dagger , in reverse order starting from the $(n+m)$ -th time slice as indicated by Eq. (23), leads to a new Slater determinant $\Phi_{m,k}$. We can stabilize $\Phi_{m,k}$ periodically until the desired value of m is reached, writing it in the UDV form and discarding D and V . This is because only $\Phi_{m,k}$ in orthonormal form is needed in the final estimator in Eq. (23), while the contribution of D and V is already properly accounted for in the use of the ‘‘retarded weight’’ $W_{n+m,k}$ or $\tilde{W}_{n+m,k}$.

The computational cost of the calculation of A_{BP} is thus of $\mathcal{O}(mM^2N)$ operations, to compute the determinant at the bra of (21), of $\mathcal{O}(M^2N) + \mathcal{O}(MN^2) + \mathcal{O}(N^3)$ operations to compute the one-body Green’s function in (23), and of $\mathcal{O}(M^2)$ operations to compute the rescaled matrix elements in (21): the additional cost of each BP segment of length m in imaginary time is approximately the same as propagating the determinants in the forward direction for m steps. In most implementations (as is the case in the present work), the auxiliary-field configurations are stored and carried during the forward direction. Hybrid procedures are possible where one stores segments of propagators during the forward direction [37], which would reduce the amount of computing but possibly with tradeoff on the memory requirement.

2. Free projection in the backward direction

As mentioned, the BP time β_{BP} is typically modest, in order to ensure sufficient number of independent paths in the BP direction. Clearly it is possible to increase the overall population size to prolong β_{BP} , however the decay in the number of independent ancestry paths is rapid and the procedure is asymptotically unstable for $\beta_{\text{BP}} \rightarrow \infty$. (This is in common with the forward walking scheme [38], on which the basic idea of BP is based.) We have not found this to be a serious limitation, in a variety of AFQMC BP calculations in strongly correlated models.

It is then reasonable to consider using a free-projection in the BP segment of the calculation. In other words, the imaginary-time propagation in the forward direction (i.e. at the ket) of Eq. (20) is performed under the usual phaseless approximation to time n , and under free-projection from n to $n+m$ so as to allow full path sampling in the backwards direction. Practically:

algorithm	forward propagation	backward propagation
	$ \Psi_{n,k}\rangle$	$\langle\Phi_{m,k} $
BP-PhL	constrained	phaseless
BP-PRes	constrained	carry $\text{Im}(E_L)$; undo cosine projection
BP-PRes (partial)	constrained	carry $\text{Im}(E_L)$
BP-FP	constrained	free projection

TABLE I. Summary of the back-propagation algorithms employing phaseless (PhL), path restoration (PRes), and free-projection (FP). In all cases, forward propagation is constrained. Backward propagation is carried out by removing, at different levels, the constraints applied in the forward direction.

1. a large number of walkers is equilibrated under the phaseless constraint
2. the constraint is released going forward for some imaginary-time segment, and back-propagation is performed on this segment.
3. points 1,2 are iterated until a desired statistical accuracy is reached.

The method brings back the phase problem, although there is a finite signal-to-noise ratio (in the spirit of a finite-temperature calculation). Its statistical errors will thus grow with N and M , unlike in BP-PhL and BP-PRes calculations, which have well-behaved polynomial computational scaling. The different BP algorithms explored in the present work are summarized in I

3. Multideterminant trial wavefunctions

For total energy calculations, the phaseless approximation has demonstrated rather weak dependence on the trial wave functions. Typically single-determinant $|\Psi_T\rangle$ has been used. In strongly correlated and/or strongly multi-reference systems, the use of multideterminants as trial wavefunctions can improve the quality and efficiency of AFQMC calculations [11, 16, 32, 39].

Formally it is straightforward to generalize the use of multideterminant trial wave function to our BP schemes. If the trial wavefunction is a linear combination

$$|\Psi_T\rangle = \sum_{\alpha} A_{\alpha} |\Psi_T^{(\alpha)}\rangle \quad (26)$$

of Slater determinants $\Psi_T^{(\alpha)}$, the state $\Phi_{m,k}$ takes the form $|\Phi_{m,k}\rangle = \sum_{\alpha} A_{\alpha} |\Phi_{m,k}^{(\alpha)}\rangle$ with

$$|\Phi_{m,k}^{(\alpha)}\rangle = \hat{B}^{\dagger}((\mathbf{x} - \bar{\mathbf{x}})_{n,k}) \dots \hat{B}^{\dagger}((\mathbf{x} - \bar{\mathbf{x}})_{n+m-1,k}) |\Psi_T^{(\alpha)}\rangle \quad (27)$$

The stabilization procedure only requires minor modification to account for the linear combination. Each determinant $\Phi_{m,k}^{(\alpha)}$ can be stabilized separately. The procedure yields a determinant $\bar{\Phi}_{m,k}^{(\alpha)}$, which comes from the

$U^{(\alpha)}$ term in the modified Gram-Schmidt decomposition. However, unlike in the case of a single determinant, the diagonal matrix $D^{(\alpha)}$ cannot be discarded, since it contributes to the relative weight:

$$|\Phi_{m,k}^{(\alpha)}\rangle = \lambda_{m,k}^{(\alpha)} |\bar{\Phi}_{m,k}^{(\alpha)}\rangle, \quad (28)$$

i.e., the coefficient $\lambda_{m,k}^{(\alpha)}$ should contain the determinant of $D^{(\alpha)}$. Correspondingly, Eq. (23) takes the form

$$\frac{\langle\Phi_{m,k}^{(\alpha)}|\hat{A}|\Psi_{n,k}\rangle}{\langle\Phi_{m,k}^{(\alpha)}|\Psi_{n,k}\rangle} = \frac{\sum_{\alpha} \xi_{n,m,k}^{(\alpha)} \frac{\langle\bar{\Phi}_{m,k}^{(\alpha)}|\hat{A}|\Psi_{n,k}\rangle}{\langle\bar{\Phi}_{m,k}^{(\alpha)}|\Psi_{n,k}\rangle}}{\sum_{\alpha} \xi_{n,m,k}^{(\alpha)}} \quad (29)$$

where $\xi_{n,m,k}^{(\alpha)} = A_{\alpha} \lambda_{m,k}^{(\alpha)} \langle\bar{\Phi}_{m,k}^{(\alpha)}|\Psi_{n,k}\rangle$, and each of the mixed Green's functions can be computed as in Eq. (23). Furthermore, to prevent numeric overflows or underflows, the amplitudes $\xi_{n,m,k}^{(\alpha)}$ can be periodically rescaled by a common factor.

The use of multideterminant trial wave functions offers a systematic route to improve the quality of the mixed and BP results. The major drawback of the multideterminant trial wave function is the so-called size extensivity: to treat the electron correlation effects consistently, the number of Slater determinants required in a typical CI expansion grows rapidly with system size. For solid-state systems, it is typically impractical while, in molecular systems, this is less of a problem. When it is computationally feasible to generate a multideterminant trial wave function giving a good description of the molecule, for example with a truncated complete active space self-consistent field (CASSCF) calculation, the computational cost to use it in AFQMC only grows linearly with the number of Slater determinants in the trial wave function. The corresponding efficiency can be even higher [11], since a better trial wave function can reduce the statistical error as well as the systematic error.

IV. RESULTS

We apply the BP algorithm to several atomic and molecular systems, primarily chosen for benchmarking purposes. Most of the AFQMC calculations reported below used a single Slater determinant from HF as trial wave function. It will be explicitly stated whenever additional tuning of the trial wave function beyond mean-field was performed. We interfaced our AFQMC code with the NWChem [40] and PySCF [41] quantum chemistry libraries to import the Gaussian one-electron and two-electron matrix elements, the overlap matrix, the trial wave function and the atomic orbitals. All of our calculations are done using the spherical harmonics representation of basis functions.

For comparison, we also employed well-established quantum chemistry methods where possible, including HF, second-order Møller-Plesset perturbation theory

(MP2), CC, CASSCF, and FCI. We performed CASSCF and FCI calculations using PySCF, and MP2 and CC calculations with NWChem. Coupled-cluster calculations are of the type RCCSD, i.e., based on the restricted HF (RHF) reference state.

A. Illustrative results and benchmark study

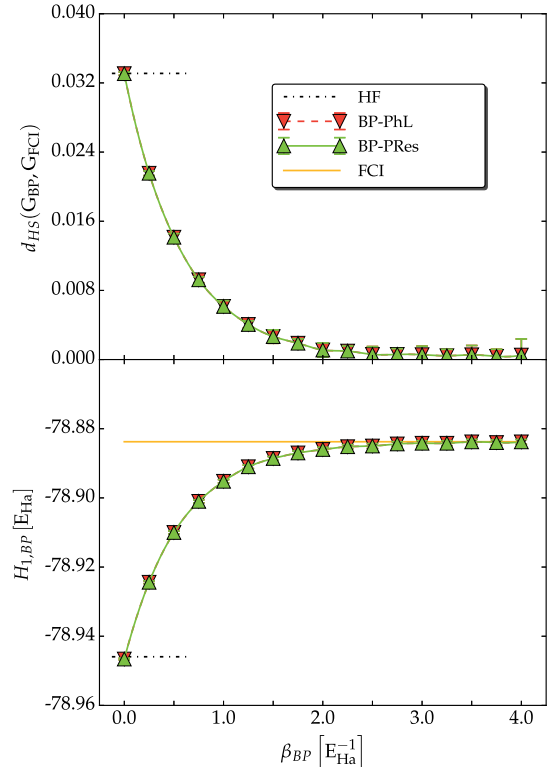


FIG. 2. (color online) Evolution of the Hilbert-Schmidt distance between G_{BP} and G_{FCI} , and of the one-electron energy $H_{1,BP}$ (bottom) with back-propagation time for CH_4 (STO-3G level, tetrahedral geometry, $R_{CH} = 1.1085 \text{ \AA}$) using BP-PhL and BP-PRes.

To study the accuracy of the BP algorithms, we compute the ground-state one-electron energy and dipole moment for several small molecules using the STO-3G and cc-pVDZ basis sets [42, 43]. The small number of electrons and atomic orbitals in these systems enable direct comparisons with FCI. We also compute the spin-averaged one-body Green’s function

$$(G_{BP})_{ij} = \frac{1}{2} \sum_{\sigma} \langle \hat{a}_{i\sigma}^{\dagger} \hat{a}_{j\sigma} \rangle_{BP}, \quad (30)$$

and measure the error with respect to FCI by the Hilbert-Schmidt distance

$$d_{HS}(G_{BP}, G_{FCI}) = \sqrt{\text{Tr}[(G_{BP} - G_{FCI})^2]}. \quad (31)$$

In Figure 2 we show the computed Green’s function and the one-electron energy in CH_4 . The simple PhL

back-propagation is seen to work well, leading to results in excellent agreement with FCI. Correspondingly, the ground-state energy computed from the mixed-estimator is $-39.8069(1) E_{Ha}$, compared to $-39.8070 E_{Ha}$ from FCI. These observations are consistent with the system being weakly interacting and little bias being incurred by the phaseless constraint imposed in the forward direction. As one would expect, the improved BP-PRes algorithm does not change the results from PhL in this case.

Figure 3 illustrates the behaviors in a pair of less straightforward systems, the Ne atom and the HeH^+ molecule. Here significant bias is seen from the PhL algorithm. The computed ground-state energies from the mixed estimate are $-128.6819(1) E_{Ha}$ (vs. -128.6809 from FCI) and $-2.9612(1) E_{Ha}$ (vs $-2.9609 E_{Ha}$ from FCI) respectively. The BP-PRes algorithm leads to a systematic and substantial improvement in both cases. To separate the contributions from the two parts in PRes, we also show here results from a partial restoration in the BP direction of the paths, by incorporating the complex phases but omitting the restoration of the cosine projection. We see that, although the phase factor tends to play the more dominant role, both components can have a non-negligible effect. This trend holds quite generally, and is consistent with the analysis in Sec. III B on the rationale for path restoration in the BP direction.

Tests conducted on 15 molecules at STO-3G, cc-pVDZ level show that the combination of the two adjustments in BP-PRes yields a systematic improvement over the PhL algorithm in all cases. The average discrepancy in the computed one-electron energies and dipole moments is reduced by $\sim 50\%$ on average, while the Hilbert-Schmidt distances for the computed Green’s functions is reduced by a factor of ~ 3 on average.

We illustrate the effect of free-projection in the back-propagation direction (BP-FP) in Figure 4. The BP-FP algorithm is seen to further reduce the small discrepancy from BP-PRes and yield essentially exact results on the Green’s function and dipole moment. The NH_3 example studied here is fairly challenging, as evidenced by the significant amount of bias shown by BP-PhL. The fact that BP-FP leads to very accurate results on the expectation values indicates that the samples $|\Psi_n(\mathbf{X})\rangle$ in Eq. (18) give an excellent representation of the ground-state wave function, despite the phaseless constraint imposed when they are generated in the forward direction. This is consistent with the fact that the ground-state energies computed by phaseless AFQMC tend to be very accurate. The main source of inaccuracy in BP-PhL is in the backward direction, in which the paths constrained in the forward direction are a poor approximation when used in reversed direction. The BP-PRes restores paths except for those terminated in the forward direction, hence the significant improvement in accuracy.

The calculations discussed thus far have used the HF state as trial wavefunctions. It is straightforward to employ a multideterminant trial wavefunction as we have discussed in Sec. III C 3. An example is shown in Fig-

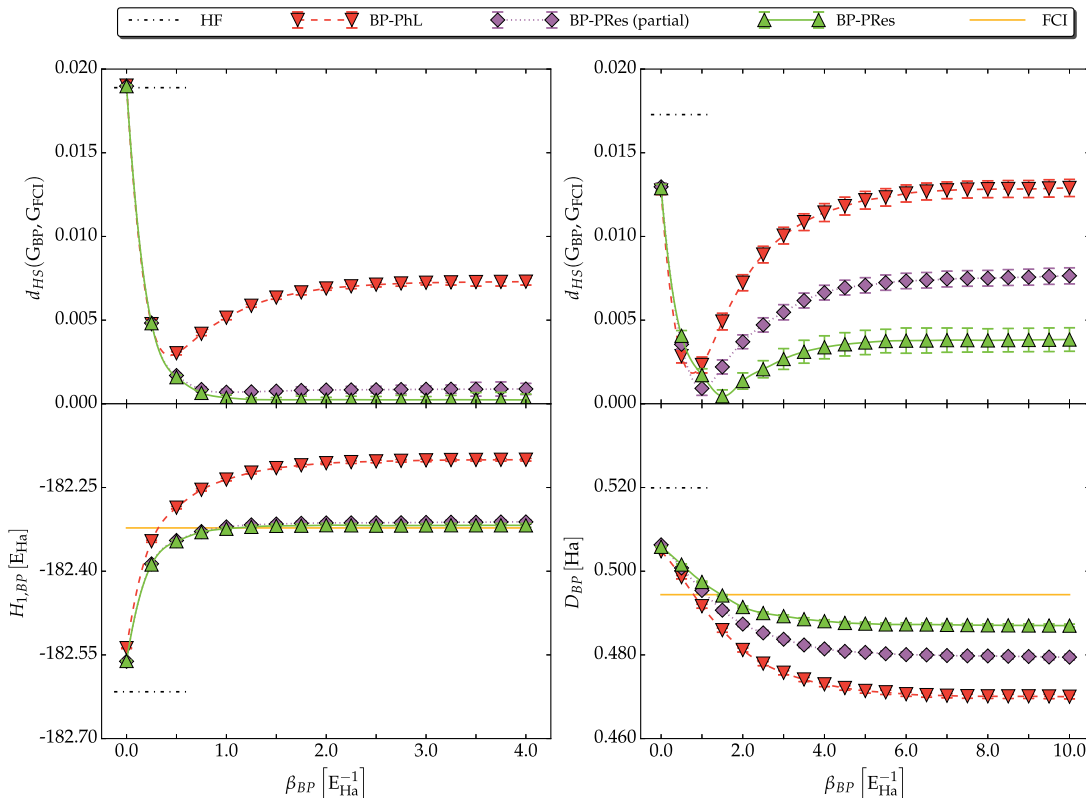


FIG. 3. (color online) Left: Evolution of the Hilbert-Schmidt distance between G_{BP} and G_{FCI} (top) and of the one-electron energy (bottom) with back-propagation time for Ne (cc-pVDZ level) using PhL and PRes back-propagation. Right: Evolution of the Hilbert-Schmidt distance between G_{BP} and G_{FCI} (top) and of the dipole moment (bottom) with back-propagation time for HeH^+ (cc-pVDZ level, $R_{\text{HeH}} = 0.79$ Å) using BP-PhL and BP-PRes. The results of a partial PRes (carrying the phase during BP but without undoing the cosine projection) are also shown.

ure 5. The computation of the dipole moment of carbon monoxide is very difficult. HF predicts the wrong sign. As a result, AFQMC with BP-PRes using HF trial wave function still retains a significant error. Using a truncated CASSCF(7,10) wavefunction as Ψ_T brings the AFQMC estimate of the dipole moment much closer to the BP-FP result (the BP-FP calculation used a simple truncated CASSCF(3,7) trial wave function). Convergence with β_{BP} is also improved, as well as the statistical accuracy. The improvement comes at the cost of a modest overhead, since the truncated CASSCF trial wavefunction in BP-PRes has a linear combination of 40 Slater determinants.

B. Application to small and medium-sized molecules

We now apply the new BP algorithm, as a first test, to compute ground-state properties of several molecules. Figure 6 shows the computed dipole moment and electronic density of H_2O at experimental equilibrium geometry [44]. The dipole moment was obtained using cc-pV x Z basis sets, with $x = 2, 3, 4, 5$. Results are extrapolated to the complete basis set limit, $x \rightarrow \infty$, using the exponen-

tial Ansatz $D(x) = \alpha + \beta e^{-\gamma x}$ [45]. AFQMC from BP-PRes using a truncated CASSCF(5,7) trial wavefunction yields a dipole moment of $D = 0.728(3)$ Ha, in agreement with the experimental result of $D = 0.7297$ Ha [46]. The computed result is seen to improve appreciably over those from both MP2 and RCCSD. We also compute the electronic density

$$\rho(\mathbf{r}) = \sum_{ij} 2 (G_{BP})_{ij} \varphi_i(\mathbf{r}) \varphi_j(\mathbf{r}), \quad (32)$$

where $\varphi_i(\mathbf{r})$ are the molecular orbitals. The results for water at the cc-pV5Z level are shown in the bottom panel in Figure 6.

Back-propagation gives access to all ground-state properties, including the two-body reduced density matrix and correlation functions of one-body operators. As an example, we compute the spin-spin correlation function

$$C(\mathbf{r}, \mathbf{r}_0) = \sum_{\alpha=1}^3 \frac{\langle \Psi_0 | \hat{S}_\alpha(\mathbf{r}_0) \hat{S}_\alpha(\mathbf{r}) | \Psi_0 \rangle}{\langle \Psi_0 | \Psi_0 \rangle} \quad (33)$$

$$\hat{S}_\alpha(\mathbf{r}) = \sum_{ij, \sigma\tau} (\sigma_\alpha)_{\sigma\tau} \varphi_i(\mathbf{r}) \varphi_j(\mathbf{r}) \hat{a}_{i\sigma}^\dagger \hat{a}_{j\tau}$$

where σ_α are Pauli matrices and φ_i, φ_j are again molecular orbitals. In Figure 7 we show results for C_6H_6 at

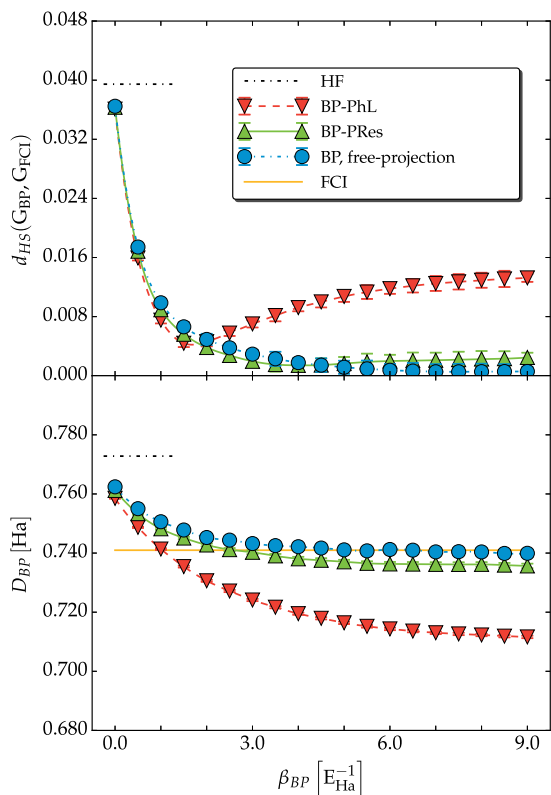


FIG. 4. (color online) Illustration of the BP-FP algorithm. Evolution of the Hilbert-Schmidt distance between G_{BP} and G_{FCI} (top) and the dipole moment (bottom) is shown versus back-propagation time. The system is NH_3 (STO-3G level, trigonal pyramid geometry, $R_{NH} = 1.07 \text{ \AA}$, $\theta_{HNH} = 100.08^\circ$).

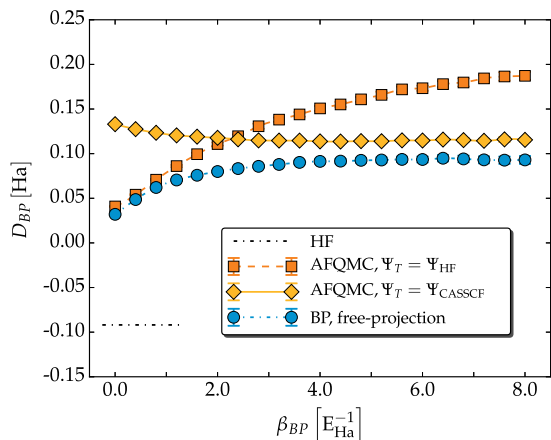


FIG. 5. (color online) Illustration of the use of multiterminal trial wave functions. Evolution of the dipole moment with back-propagation time is shown for CO (cc-pVDZ level, $R_{CO} = 1.1282 \text{ \AA}$) using BP-PRes guided by a truncated CASSCF wavefunction (yellow diamonds). Results are compared to those from BP-FP (blue circles). The corresponding BP-PRes with RHF is also shown (orange squares) for reference.

experimental equilibrium geometry [47] (specified by the

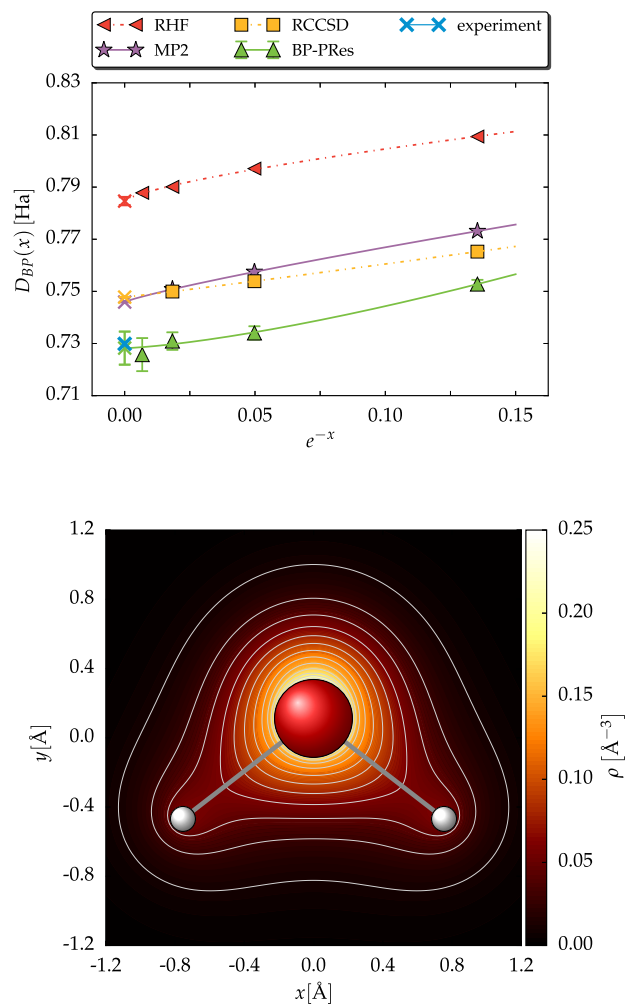


FIG. 6. (color online) Top: Computed dipole moment of H_2O at the experimental equilibrium geometry, using cc-pV x Z bases, with $x = 2, 3, 4, 5$, and the extrapolation to the complete basis set limit. The corresponding results from RHF, MP2, and RCCSD are also shown. Bottom: Computed electronic density of H_2O by AFQMC along the molecular plane, at the cc-pV5Z level.

radii $R_C = 1.397 \text{ \AA}$, $R_H = 2.481 \text{ \AA}$ of the C and H rings, respectively.) The figure shows the correlation function in Eq. (33) for $\mathbf{r}_0 = (x_0, y_0, z_0) = (0, R_C, 0.5)$ Bohr, and $\mathbf{r} = (x, y, z_0)$. This choice corresponds to placing a reference spin above one of the C atoms and showing the correlation function in the plane parallel to the molecule. Here we used a truncated CASSCF(5,20) state as trial wavefunction. The alternation between positive and negative values (warm and cold colours) suggests the presence of antiferromagnetic correlations along the C bonds. Correspondingly a correlation is also present along each CH bonds.

Finally we compute the dipole moments of a few organic molecules (ethanol CH_3CH_2OH , formic acid $HCOOH$, acetic acid CH_3COOH , propionic acid CH_3CH_2COOH) in their most stable conformer (trans,

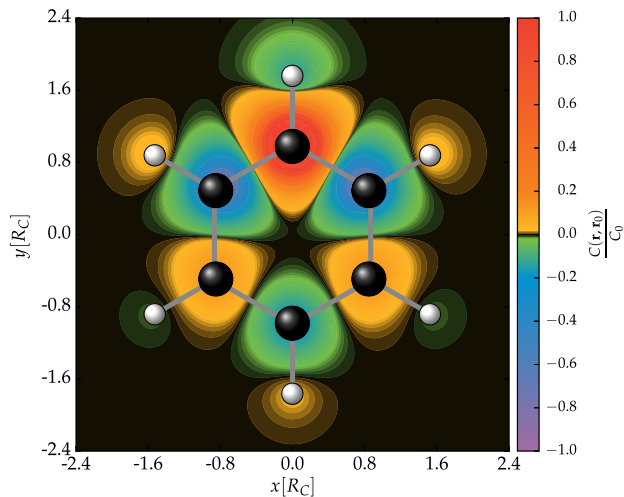


FIG. 7. (color online) Spin-spin correlation function, $C(\mathbf{r}, \mathbf{r}_0)$, of benzene at experimental equilibrium geometry, computed by AFQMC with BP-PRes in the STO-6G basis. The correlation function is shown for $\mathbf{r} = (x, y, z_0)$, i.e., in a plane parallel with the molecule at a distance $z_0 = 0.5$ Bohr above, with the reference spin placed in the same plane directly on top of a C atom (the one with the highest y value in the figure). $C(x, y)$ is normalized by the magnitude $C_0 = |\min_{x,y} C(x, y)|$ of the most negative value, and capped above C_0 .

trans, syn, T_t), at 6-31G* level. We employ the experimental equilibrium geometries for $\text{CH}_3\text{CH}_2\text{OH}$ [48] and HCOOH [47] and the CCSD, CCSD(T) equilibrium geometries [49] for CH_3COOH and $\text{CH}_3\text{CH}_2\text{COOH}$ respectively. As seen in Figure 8, the AFQMC results with BP-PRes are generally in good agreement with those from RCCSD. When a discrepancy is evident, the BP-FP result falls closer to that of BP-PRes.

These studies can be carried out beyond the 6-31G* level, as shown in Figure 9 using $\text{CH}_3\text{CH}_2\text{OH}$ as test case. AFQMC results are converged to the CBS limit, and lie roughly two joint error bars away from experiment [49].

Given the favorable computational scaling of AFQMC, this is encouraging indication that the method can potentially provide an accurate description of electronic prop-

erties in molecules containing hydroxyl, carboxyl and methyl functional groups.

V. CONCLUSIONS

In the present work we have focused on developing the AFQMC method for many-body computations in molecules and solids beyond the total energy. We investigated the use of back-propagation to compute ground-state observables and correlation functions. We proposed an algorithm which allows path restoration in the back-propagation (BP-PRes) for cases when the phaseless constraint is invoked to control the phase problem. The algorithm was tested against exact diagonalization and other reference quantum chemistry methods in molecules from the first two rows of the periodic table. We find that significant improvement is achieved with BP-PRes in molecules and solids, where a phase problem is always present in AFQMC, over the simple BP scheme applied in systems with “only” a sign problem.

Results are obtained on various quantities including the dipole moment, density matrix, and spin-spin correlation functions. These results indicate that AFQMC can become an accurate tool to calculate not only total energy, but all ground-state properties of molecules and real materials. We hope that this advance will encourage further development and application of the methodology to real materials.

VI. ACKNOWLEDGMENTS

We thank W. A. Al-Saidi for his contribution at early stages of the project, and H. Krakauer and F. Ma for collaborations and discussions. M. M. acknowledges Q. Sun and G. K.-L. Chan for help in understanding and using PySCF. We acknowledge support by NSF (Grant no. DMR-1409510) and the Simons Foundation. Computations were carried out at the Extreme Science and Engineering Discovery Environment (XSEDE), which is supported by National Science Foundation grant number ACI-1053575, and at the Storm and SciClone Clusters at the College of William and Mary.

-
- [1] A. Szabo and N. Ostlund, *Modern Quantum Chemistry: Introduction to Advanced Electronic Structure Theory*. Dover Books on Chemistry, Dover Publications, 1996.
- [2] R. J. Bartlett and M. Musiał, “Coupled-cluster theory in quantum chemistry,” *Rev. Mod. Phys.*, vol. 79, pp. 291–352, Feb 2007.
- [3] B. Hammond, W. Lester, and P. Reynolds, *Monte Carlo Methods in Ab Initio Quantum Chemistry*. Lecture and Course Notes In Chemistry Series, World Scientific, 1994.
- [4] W. M. C. Foulkes, L. Mitas, R. J. Needs, and G. Rajagopal, “Quantum Monte Carlo simulations of solids,” *Rev. Mod. Phys.*, vol. 73, pp. 33–83, Jan 2001.
- [5] K. P. Esler, J. Kim, D. M. Ceperley, W. Purwanto, E. J. Walter, H. Krakauer, S. Zhang, P. R. C. Kent, R. G. Hennig, C. Umrigar, M. Bajdich, J. Kolerenc, L. Mitas, and A. Srinivasan, “Quantum Monte Carlo algorithms for electronic structure at the petascale; the endstation project,” *Journal of Physics: Conference Series*, vol. 125, no. 1, p. 012057, 2008.
- [6] M. Motta, D. M. Ceperley, G. K.-L. Chan, L. A. Gomez, E. Gull, S. Guo, C. Jimenez-Hoyos, T. N. Lan, J. Li, F. Ma, A. J. Millis, N. Prokof’ev, U. Ray, G. E. Scuseria,

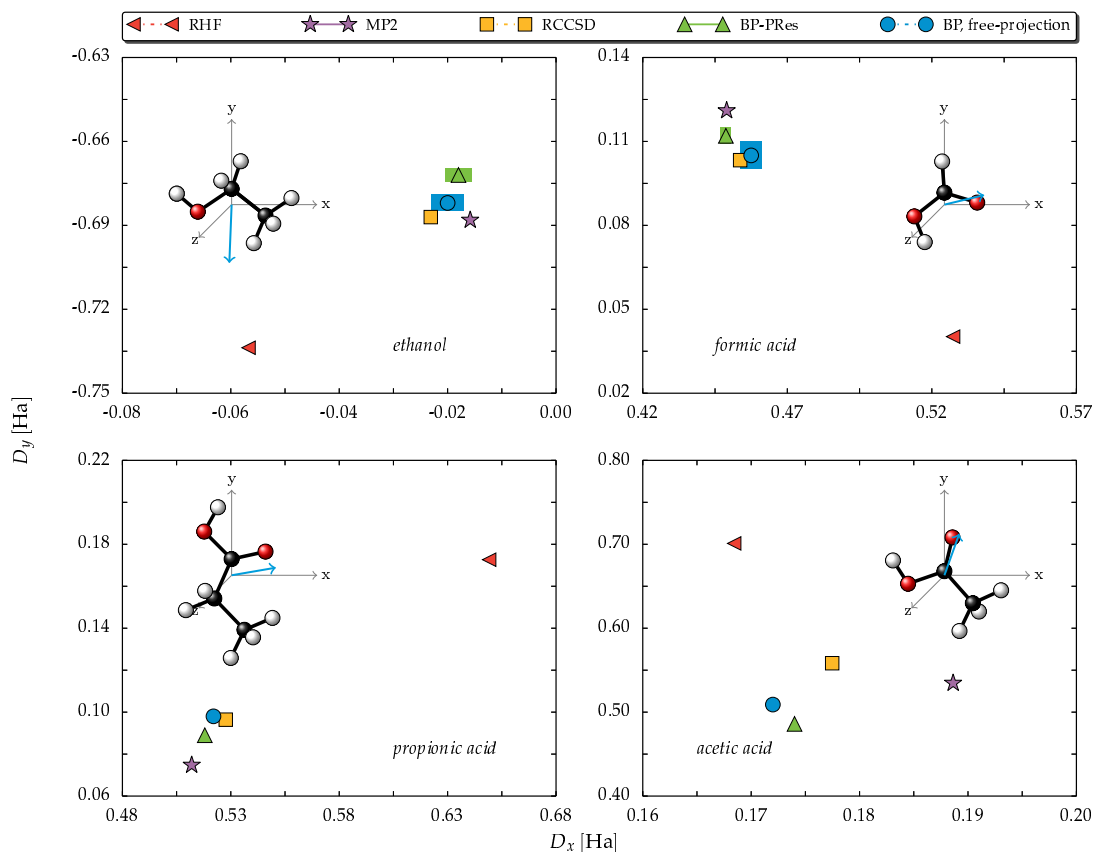


FIG. 8. (color online) Computed dipole moments from AFQMC with BP-PRes for some medium-sized organic molecules (6-31G* basis). Results for RHF, MP2, and RCCSD are also shown for reference. Molecular geometries and AFQMC dipoles based on the free-projection scheme are sketched in each panel (in all cases, in the chosen frame of reference D_z is equal to or statistically compatible with 0, as expected for these C_s symmetric molecules).

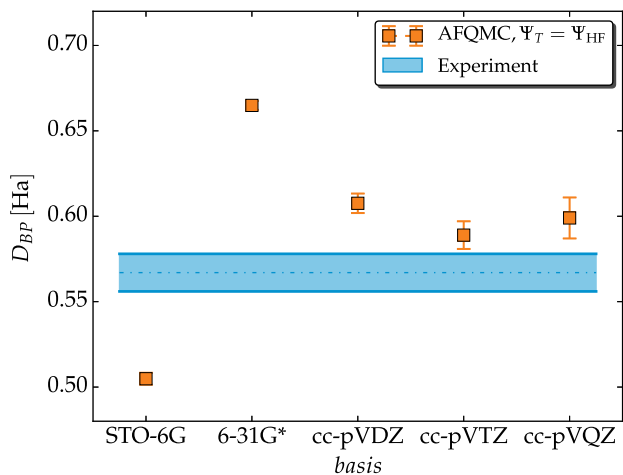


FIG. 9. (color online) Computed dipole moment from AFQMC with BP-PRes, for trans-ethanol at STO-6G to cc-pVQZ level. Experimental dipole moment is shown for reference.

S. Sorella, E. M. Stoudenmire, Q. Sun, I. S. Tupytin, S. R. White, D. Zgid, , and S. Zhang, “Towards the so-

lution of the many-electron problem in real materials: equation of state of the hydrogen chain with state-of-the-art many-body methods,” *arXiv:1705.01608*, 2017.

- [7] E. Y. Loh, J. E. Gubernatis, R. T. Scalettar, S. R. White, D. J. Scalapino, and R. L. Sugar, “Sign problem in the numerical simulation of many-electron systems,” *Phys. Rev. B*, vol. 41, pp. 9301–9307, May 1990.
- [8] P. J. Reynolds, D. M. Ceperley, B. J. Alder, and W. A. L. Jr., “Fixed-node quantum Monte Carlo for molecules,” *The Journal of Chemical Physics*, vol. 77, no. 11, pp. 5593–5603, 1982.
- [9] S. Zhang and H. Krakauer, “Quantum Monte Carlo method using phase-free random walks with Slater determinants,” *Phys. Rev. Lett.*, vol. 90, p. 136401, Apr 2003.
- [10] W. A. Al-Saidi, S. Zhang, and H. Krakauer, “Auxiliary-field quantum Monte Carlo calculations of molecular systems with a gaussian basis,” *The Journal of Chemical Physics*, vol. 124, no. 22, p. 224101, 2006.
- [11] W. A. Al-Saidi, S. Zhang, and H. Krakauer, “Bond breaking with auxiliary-field quantum Monte Carlo,” *The Journal of Chemical Physics*, vol. 127, no. 14, p. 144101, 2007.
- [12] M. Suewattana, W. Purwanto, S. Zhang, H. Krakauer, and E. J. Walter, “Phaseless auxiliary-field quantum Monte Carlo calculations with plane waves and pseu-

- dopotentials: Applications to atoms and molecules,” *Phys. Rev. B*, vol. 75, p. 245123, Jun 2007.
- [13] W. Purwanto, W. A. Al-Saidi, H. Krakauer, and S. Zhang, “Eliminating spin contamination in auxiliary-field quantum Monte Carlo: Realistic potential energy curve of F_2 ,” *The Journal of Chemical Physics*, vol. 128, no. 11, p. 114309, 2008.
- [14] W. Purwanto, H. Krakauer, and S. Zhang, “Pressure-induced diamond to β -tin transition in bulk silicon: A quantum Monte Carlo study,” *Phys. Rev. B*, vol. 80, p. 214116, Dec 2009.
- [15] W. Purwanto, H. Krakauer, Y. Virgus, and S. Zhang, “Assessing weak hydrogen binding on Ca^+ centers: An accurate many-body study with large basis sets,” *The Journal of Chemical Physics*, vol. 135, no. 16, p. 164105, 2011.
- [16] W. Purwanto, S. Zhang, and H. Krakauer, “Auxiliary-field quantum Monte Carlo calculations of the molybdenum dimer,” *The Journal of Chemical Physics*, vol. 144, no. 24, p. 244306, 2016.
- [17] J. Shee, S. Zhang, D. R. Reichman, and R. A. Friesner, “Chemical transformations approaching chemical accuracy via correlated sampling in auxiliary-field quantum Monte Carlo,” *Journal of Chemical Theory and Computation*, vol. 13, no. 6, pp. 2667–2680, 2017. PMID: 28481546.
- [18] J. P. F. LeBlanc, A. E. Antipov, F. Becca, I. W. Bulik, G. K.-L. Chan, C.-M. Chung, Y. Deng, M. Ferrero, T. M. Henderson, C. A. Jiménez-Hoyos, E. Kozik, X.-W. Liu, A. J. Millis, N. V. Prokof’ev, M. Qin, G. E. Scuseria, H. Shi, B. V. Svistunov, L. F. Tocchio, I. S. Tupitsyn, S. R. White, S. Zhang, B.-X. Zheng, Z. Zhu, and E. Gull, “Solutions of the two-dimensional Hubbard model: Benchmarks and results from a wide range of numerical algorithms,” *Phys. Rev. X*, vol. 5, p. 041041, Dec 2015.
- [19] M. Qin, H. Shi, and S. Zhang, “Coupling quantum Monte Carlo and independent-particle calculations: Self-consistent constraint for the sign problem based on the density or the density matrix,” *Phys. Rev. B*, vol. 94, p. 235119, Dec 2016.
- [20] B.-X. Zheng, C.-M. Chung, P. Corboz, G. Ehlers, R. M. Noack, H. Shi, S. R. White, S. Zhang, and G. K.-L. Chan, “Stripe order in the underdoped region of the two-dimensional Hubbard model,” *arXiv:1701.00054*, 2017.
- [21] S. Zhang, J. Carlson, and J. E. Gubernatis, “Constrained path Monte Carlo method for fermion ground states,” *Phys. Rev. B*, vol. 55, pp. 7464–7477, Mar 1997.
- [22] W. Purwanto and S. Zhang, “Quantum Monte Carlo method for the ground state of many-boson systems,” *Phys. Rev. E*, vol. 70, p. 056702, Nov 2004.
- [23] S. Zhang, *Auxiliary-field quantum Monte Carlo for correlated electron systems*. Forschungszentrum Jülich, Inst. for Advanced Simulation, 3 ed., 2013.
- [24] F. Ma, W. Purwanto, S. Zhang, and H. Krakauer, “Quantum Monte Carlo calculations in solids with downfolded hamiltonians,” *Phys. Rev. Lett.*, vol. 114, p. 226401, Jun 2015.
- [25] H. F. Trotter, “On the product of semi-groups of operators,” *Proc. Amer. Math. Soc.*, vol. 10, p. 545, 1959.
- [26] M. Suzuki, “Generalized Trotter’s formula and systematic approximants of exponential operators and inner derivations with applications to many-body problems,” *Comm. Math. Phys.*, vol. 51, no. 2, pp. 183–190, 1976.
- [27] R. L. Stratonovich, “On a method of calculating quantum distribution functions,” *Soviet Physics Doklady*, vol. 2, p. 416, July 1957.
- [28] J. Hubbard, “Calculation of partition functions,” *Phys. Rev. Lett.*, vol. 3, pp. 77–78, Jul 1959.
- [29] H. Shi and S. Zhang, “Symmetry in auxiliary-field quantum Monte Carlo calculations,” *Phys. Rev. B*, vol. 88, p. 125132, Sep 2013.
- [30] S. Zhang, H. Krakauer, W. A. Al-Saidi, and M. Suewattana, “Quantum simulations of realistic systems by auxiliary fields,” *Computer Physics Communications*, vol. 169, no. 1, pp. 394 – 399, 2005. Proceedings of the Europhysics Conference on Computational Physics 2004.
- [31] W. Purwanto and S. Zhang, “Correlation effects in the ground state of trapped atomic Bose gases,” *Phys. Rev. A*, vol. 72, p. 053610, Nov 2005.
- [32] W. Purwanto, S. Zhang, and H. Krakauer, “An auxiliary-field quantum Monte Carlo study of the chromium dimer,” *The Journal of Chemical Physics*, vol. 142, no. 6, p. 064302, 2015.
- [33] Y. Virgus, W. Purwanto, H. Krakauer, and S. Zhang, “Stability, energetics, and magnetic states of cobalt adatoms on graphene,” *Phys. Rev. Lett.*, vol. 113, p. 175502, Oct 2014.
- [34] M. Motta, D. E. Galli, S. Moroni, and E. Vitali, “Imaginary-time correlations and the phaseless auxiliary field quantum Monte Carlo,” *The Journal of Chemical Physics*, vol. 140, no. 2, p. 024107, 2014.
- [35] M. Motta, D. E. Galli, S. Moroni, and E. Vitali, “Imaginary-time density-density correlations for two-dimensional electron gases at high density,” *The Journal of Chemical Physics*, vol. 143, no. 16, p. 164108, 2015.
- [36] C.-C. Chang and S. Zhang, “Spatially inhomogeneous phase in the two-dimensional repulsive Hubbard model,” *Phys. Rev. B*, vol. 78, p. 165101, Oct 2008.
- [37] E. Vitali, H. Shi, M. Qin, and S. Zhang, “Computation of dynamical correlation functions for many-fermion systems with auxiliary-field quantum Monte Carlo,” *Phys. Rev. B*, vol. 94, p. 085140, Aug 2016.
- [38] K. S. Liu, M. H. Kalos, and G. V. Chester, “Quantum hard spheres in a channel,” *Phys. Rev. A*, vol. 10, pp. 303–308, Jul 1974.
- [39] W. Purwanto, S. Zhang, and H. Krakauer, “Excited state calculations using phaseless auxiliary-field quantum Monte Carlo: Potential energy curves of low-lying C_2 singlet states,” *The Journal of Chemical Physics*, vol. 130, no. 9, p. 094107, 2009.
- [40] M. Valiev, E. Bylaska, N. Govind, K. Kowalski, T. Straatsma, H. V. Dam, D. Wang, J. Nieplocha, E. Apra, T. Windus, and W. de Jong, “NWChem: A comprehensive and scalable open-source solution for large scale molecular simulations,” *Computer Physics Communications*, vol. 181, no. 9, pp. 1477 – 1489, 2010.
- [41] Q. Sun, T. C. Berkelbach, N. S. Blunt, G. H. Booth, S. Guo, Z. Li, J. Liu, J. McClain, E. R. Sayfutyarova, S. Sharma, S. Wouters, and G. K.-L. Chan, “The python-based simulations of chemistry framework (PySCF),” *arXiv:1701.08223*, 2017.
- [42] W. J. Hehre, R. F. Stewart, and J. A. Pople, “Self-consistent molecular-orbital methods. I. Use of gaussian expansions of Slater-type atomic orbitals,” *The Journal of Chemical Physics*, vol. 51, no. 6, pp. 2657–2664, 1969.
- [43] T. H. Dunning, “Gaussian basis sets for use in correlated molecular calculations. I. the atoms Boron through

- Neon and Hydrogen,” *The Journal of Chemical Physics*, vol. 90, no. 2, pp. 1007–1023, 1989.
- [44] A. Hoy and P. Bunker, “A precise solution of the rotation bending Schrödinger equation for a triatomic molecule with application to the water molecule,” *Journal of Molecular Spectroscopy*, vol. 74, no. 1, pp. 1 – 8, 1979.
- [45] D. Feller, “Application of systematic sequences of wave functions to the water dimer,” *The Journal of Chemical Physics*, vol. 96, no. 8, pp. 6104–6114, 1992.
- [46] D. Lide, *CRC Handbook of Chemistry and Physics, 84th Edition*. CRC Handbook of Chemistry and Physics, Taylor & Francis, 2003.
- [47] G. Herzberg, *Electronic Spectra and Electronic Structure of Polyatomic Molecules*. Electronic Spectra and Electronic Structure of Polyatomic Molecules, Krieger Publishing Company, 1991.
- [48] S. Coussan, Y. Bouteiller, J. P. Perchard, and W. Q. Zheng, “Rotational isomerism of ethanol and matrix isolation infrared spectroscopy,” *The Journal of Physical Chemistry A*, vol. 102, no. 29, pp. 5789–5793, 1998.
- [49] R. D. J. III, *NIST Computational Chemistry Comparison and Benchmark Database (CCC-BDB)*. NIST Standard Reference Database Number 101, Release 18, 2016.